LOCAL ISOLATION OF MICROSCALE DEFECTIVE AREAS IN MONOCRYSLINE SILICON SOLAR CELLS

Adam Gajdos

Doctoral Degree Programme (2), FEEC BUT

E-mail: xgajdo12@stud.feec.vutbr.cz

Supervised by: Pavel Skarvada

E-mail: skarvada@feec.vutbr.cz

Abstract: This article is aimed on characterization of silicon solar cells microstructural inhomogeneities. To detect inhomogeneity or imperfection, reverse biased current voltage (*I-V*) measurement is used. These imperfections in some cases may cause avalanche type of breakdown, that can be visible in *I-V* curve. Therefore, the fact that certain imperfections emit light is used for localization needs. Raw localization is provided by electroluminescence (EL) method. Near-field scanning microscopy (SNOM) combined with photomultiplier tube is used for microscale localization. Both methods are done in reverse bias. Isolation of inhomogeneity by focused ion beam (FIB) is avoiding leakage current flow through it.

Keywords: Solar cell, FIB, SEM, SNOM, silicon, electroluminescence

1 INTRODUCTION

In these days, silicon solar cells are still the most widespread photovoltaic devices to convert solar energy to electrical one, due to long term evolution since 20th century [1]. Furthermore, silicon solar cells have one of the highest conversion efficiency in single junction except of GaAs solar cells [2]. However, numerous types of imperfections during the fabrication process may appear, such as inclusions, Schotky type shunts, cracks, crystal defects or metal contamination in some of them [3,4] . Origin of these imperfections also can be caused by mechanical stress. As a result, reliability and life time of solar cells could be impacted by these imperfections. Many of these imperfections can be eliminated by various methods. Most of imperfections are located on the edges of the solar cell and mostly they are Schotky type shunts, so it is important step to isolate edges. As a common technique in industry this shunt is removed by plasma etching of the wafer stack. Other techniques e.g. the grinding of the wafer edge with sandpaper, the cutting of isolation trenches with a wafer dicing saw and the laser separation by inserting trenches [5,6]. Other experimental method used for isolation is using FIB for milling barrier around microstructural defects [7]. This processing method provides decrease of shunt resistance in reverse biased conditions.

2 EXPERIMENTAL SYSTEMS

2.1 CURRENT VOLTAGE MEASUREMENT SET-UP

Measurements of *I-V* characteristics is performed by a source meter Keithley 2420 in thermally insulated box, which also provides basic shielding. Solar cell sample is placed between two electrodes with isolation layer in the middle to avoid electrical shunt. Thermal stability is realized by Peltier's module cooled by water circuit, module is controlled by a source meter Keithley 2510-AT. Setup is controlled by PC via GPIB-USB interface and it allows fully automated measurement. This basic measurement had to be done for a detection of imperfection as well as an estimation of a suitable voltage bias which essential for next presented methods.

2.2 MACROSCALE LOCALIZATION SET-UP

Experimental set-up for macroscale imperfection localization is based on a CCD camera equipped by cooled 3.2MPx Si-chip which sensing radiation in a spectral range from 300 nm to 1100 nm. Surface of solar cell is captured through macro lens with focal length 105 mm from minimum focusing distance 41 cm. Measurement is done in dark place, because the radiation from sample has very low intensity and it could not be visible in the daylight. Consequently, measurement is depended on voltage bias, because imperfection radiate from threshold level in reverse biased condition (determined by *I-V* measurement). A voltage bias is set by power supply Agilent E3631A.

2.3 MICROSCALE LOCALIZATION SET-UP

Precise localization of imperfections is performed by SNOM combined with photomultiplier tube as well in reverse biased conditions. Principle of this method is scanning surface of defective area by scanning probe and simultaneously detect the emitted radiation from imperfection by photomultiplier tube [8]. Nevertheless, radiation is glowing to all directions, thus scanning probe is placed between emitting spot and tube. While probe is scanning, amount of detected light by tube is affected. Emitted radiation is measured at each step of probe trajectory and as a result, probe forms a shadow map of defective area. Final topography with "shadow maps" is presented at Figure 2.

2.4 DEFECT-ISOLATION METHOD

To isolate microscopic imperfections dual-beam system (FIB-SEM) Tescan Lyra3 is used. Localization of defective is possible, because of the know topography provided by SNOM. Localization only by SEM would be very difficult, since there are many microscopic inhomogeneities without effect on electrical properties of the solar cell. Even back-scattered electron (BSE) detector does not provide satisfying material contrast to enable microscopic localization of defective area. Isolation process is performed by ions of gallium that mill the potential barrier around the imperfection to avoid the leakage current flow through it. Isolation barrier is in order of tens micrometers.

3 PREPARED SAMPLES AND RESULTS

Mentioned characterization and isolation methods have been done on multiple samples, but in this article only result from one sample are presented. For investigation purpose the monocrystalline silicon solar cell is cut into small pieces (approximately 10 x 10 mm^2) containing only few imperfections. Presented sample contains numerous imperfections, that provides parasitic current pathways which caused leakage current through the solar cell. A significant leakage current could be observed above the threshold reverse voltage bias $U_r > 6$ V from the red *I-V* characteristics before isolation process shown in Figure 1. Every measurement was performed several times for a stability verification and time independence of the obtained results.

A sensitive CCD camera were used for raw localization process of imperfections on cell sample. Dominant radiation was observed from spot marked as "A" in Figure 3a when reverse bias reached voltage 6 V. However, silicon does not produce visible radiation by common recombination process, visible radiation can be observed during avalanche or Zener breakdown [8]. Topography and "shadow map" of radiation spot "A" performed by SNOM with photomultiplier tube in reverse bias higher than 6 V is shown in Figure 2a. Combination of these two images provides location of radiation spot "A". Imperfection related to radiation spot "A" founded by SEM (shown in Figure 4a) is common type of defect in monocrystalline silicon devices called pit defect [9]. The breakdown mechanism of this defect type is determined as avalanche type. This defect was successfully isolated by 2 μm wide square barrier to depth of 1 μm with edge length 20 μm. As a result, formed barrier prevents current flow directed to defect. Repeated *I-V* measurement (blue, Figure 1) after defect "A" isolation shows that reverse current above breakdown voltage significantly decreased. Addition of parallel shunt resistance from fitted data for defect "A" is $R_{defA} = 2083\ \Omega$.

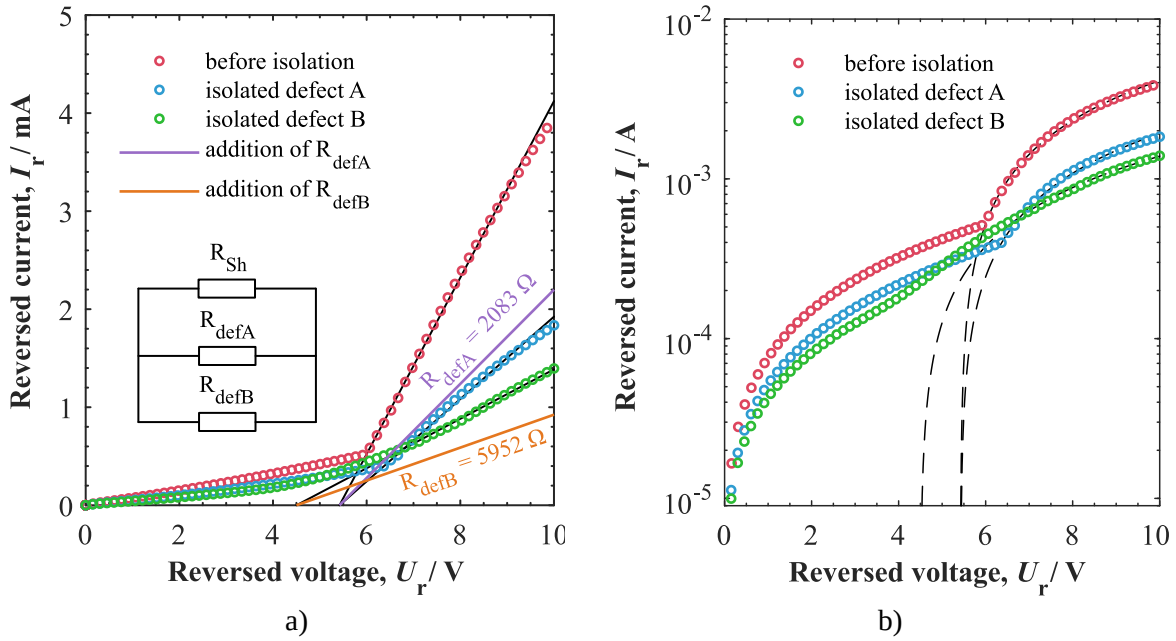

Figure 1: Current voltage curves "before" and "after" defects isolation in a) linear and b) semilogarithmic. Shunt resistance of each defect is also presented. T = 298 K.

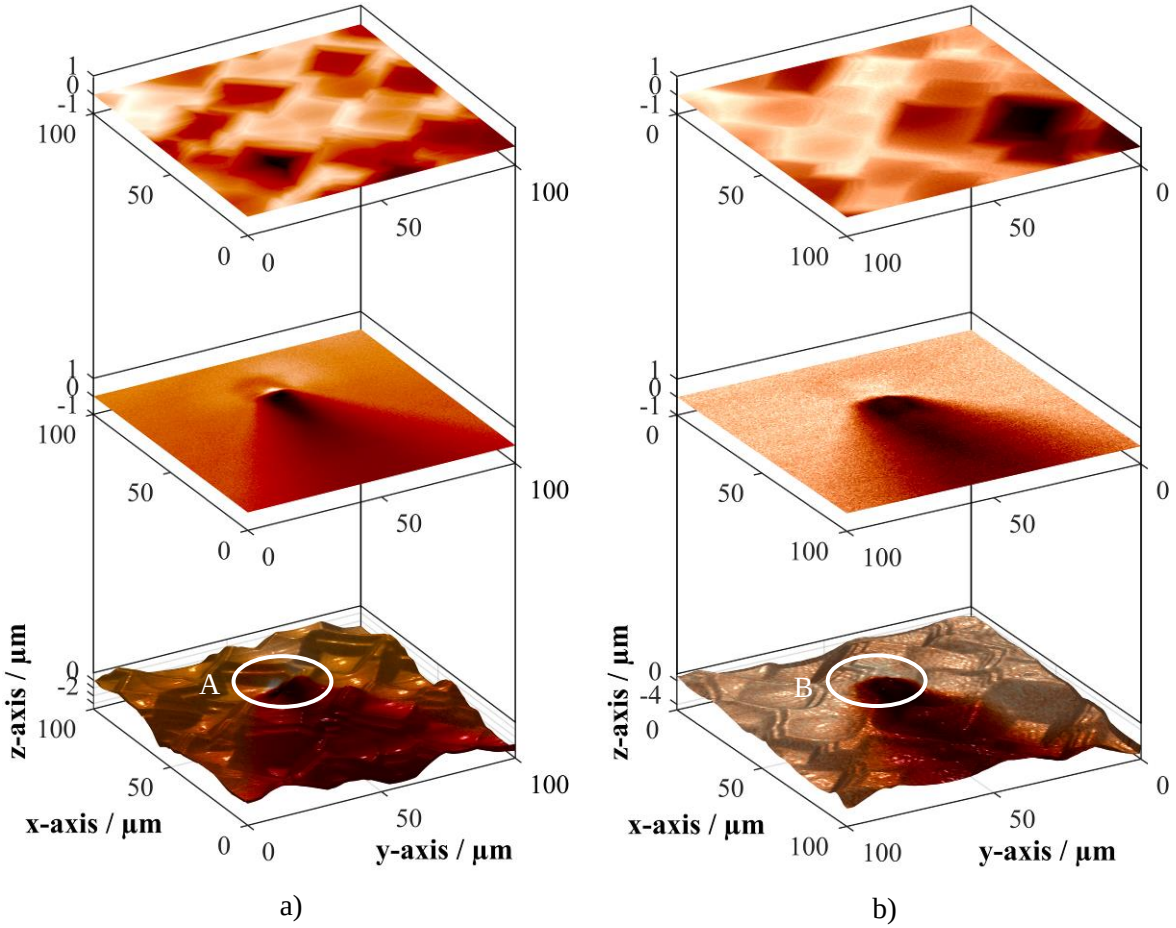

Figure 2: Topography of defective area combined with "shadow map" for a) defect A (U_r = 6.1 V) b) defect B (U_r = 6.7 V).

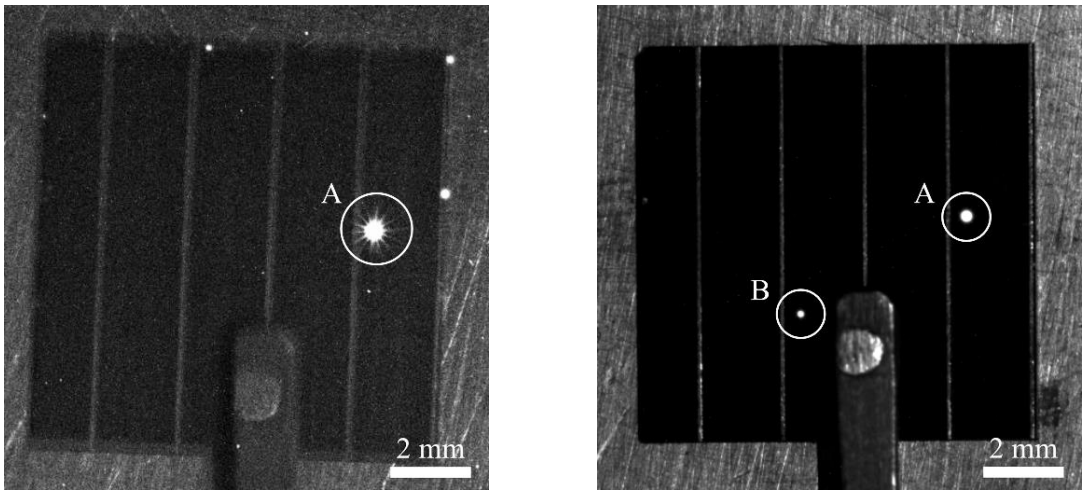

a) b)

Figure 3: a) Radiation map of defect A before isolation (U_r = 6.1 V, t = 300 s, T = 301 K), b) Radiation map overlapped on solar cell sample image before defect B isolation (U_r = 6.7 V, t = 100 s, T = 300 K).

Even if reverse current significantly decreased after defect "A" isolation, repeated measurement of the radiation shows that spot "A" still produces radiation, when bias is higher than $U_r > 6.5$ V. Moreover, Figure 3b shows minor radiation spot "B" appeared above reverse bias $U_r > 6.7$ V. The value of the breakdown voltage coincides with threshold value for radiation of spot "B". Topography of radiation spot "B" with "shadow map" is presented in Figure 2b. Corresponding SEM micrograph of defective area to topography is in Figure 4b and it is visible that radiation spot "B" is also pit type with avalanche breakdown mechanism. Defect "B" size is approximately twice smaller than defect "A".

Defect "B" was isolated by annulus with outer radius R = 14 μm and inner radius r = 12 μm milled to a depth of 2 μm in surface and successfully form a barrier for current flow directed to defect. Radiation intensity from defect "B" rapidly decreased after isolation. Decrease of reverse current after threshold voltage despite radiation intensity decrease, it is not as significant as in case of defect "A" isolation, due to other parasitic current pathways. Addition of parallel shunt resistance from fitted data for defect "B" is R_{defB} = 5952 Ω.

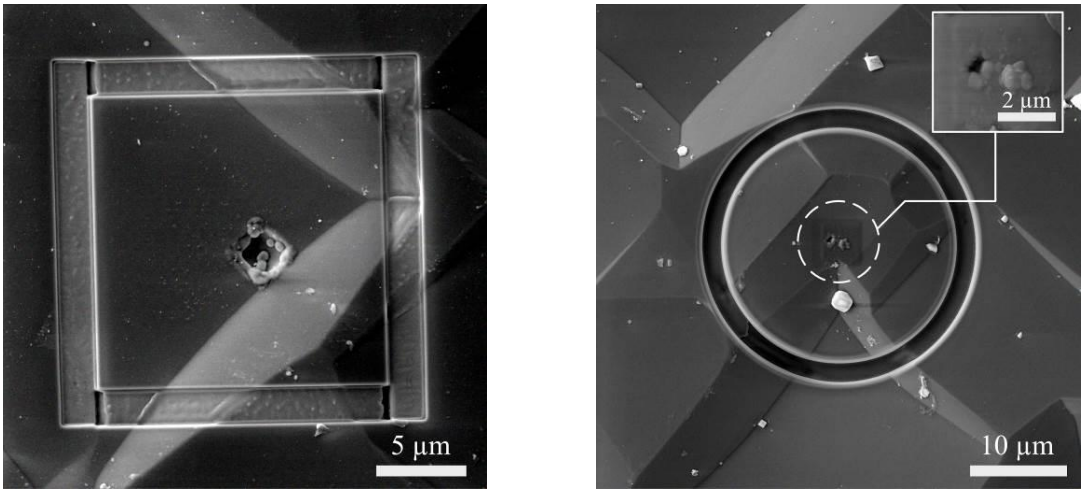

a) b)

Figure 4: SEM micrograph of isolated a) defect A and b) defect B. U_{HV} = 5 kV, detector SE, tilt 0°.

4 CONCLUSION

The methods in this paper present the measurements for a detection and localization of the defects or inhomogeneities in the silicon solar cells. These methods could be applied as well on the different types of solar cells. Result from two localized defects on one sample are presented. Breakdown voltage in *I-V* characteristics strongly correlates with radiation threshold voltage obtained by electroluminescence. Both of defects are isolated by experimental method using gallium ion milling. The process of FIB isolation has been successfully repeated on multiple solar cells samples. Electrical properties in reverse biased conditions of investigated sample has been improved. Parallel shunt resistance significantly decreased with each defect isolation.

ACKNOWLEDGEMENT

This work was supported by the Internal Grant Agency of Brno University of Technology, grant No. FEKT-S-17-4626. This support was gratefully acknowledged.

REFERENCES

[1] Green M A 2009 The path to 25% silicon solar cell efficiency: History of silicon cell evolution *Progress in Photovoltaics: Research and Applications* **17** 183–9

[2] Green M A, Hishikawa Y, Dunlop E D, Levi D H, Hohl-Ebinger J and Ho-Baillie A W Y 2018 Solar cell efficiency tables (version 51) *Prog Photovolt Res Appl* **26** 3–12

[3] Riepe S, Reis I E, Kwapil W, Falkenberg M A, Schön J, Behnken H, Bauer J, Kreßner-Kiel D, Seifert W and Koch W 2011 Research on efficiency limiting defects and defect engineering in silicon solar cells - results of the German research cluster SolarFocus *Phys. Status Solidi (c)* **8** 733–8

[4] Lausch D, Petter K, Bakowskie R, Czekalla C, Lenzner J, von Wenckstern H and Grundmann M 2010 Identification of pre-breakdown mechanism of silicon solar cells at low reverse voltages *Appl. Phys. Lett.* **97** 073506

[5] Hauser A, Hahn G, Spiegel M, Feist H, Breitenstein O, Rakotoniaina J P, Fath P and Bucher E 2001 Comparison of different techniques for edge isolation *17th European Photovoltaic Solar Energy Conference, WIP-ETA, 1739-1742 (2002)*

[6] Chan C, Abbott M, Hallam B, Juhl M, Lin D, Li Z, Li Y, Rodriguez J and Wenham S 2015 Edge isolation of solar cells using laser doping *Solar Energy Materials and Solar Cells* **132** 535–43

[7] Gajdoš A, Škvarenina L, Škarvada P and Macků R 2017 Microscale localization and isolation of light emitting imperfections in monocrystalline silicon solar cells *Photonics, Devices, and Systems VII* Photonics, Devices, and Systems VII vol 10603 (International Society for Optics and Photonics) p 1060316

[8] Škarvada P, Tománek P, Koktavý P, Macků R, Šicner J, Vondra M, Dallaeva D, Smith S and Grmela L 2014 A variety of microstructural defects in crystalline silicon solar cells *Applied Surface Science* **312** 50–6

[9] Bishop J W 1989 Microplasma breakdown and hot-spots in silicon solar cells *Solar Cells* **26** 335–49